Coercivity enhancement of sintered Nd–Fe–B magnets by grain boundary diffusion with $Pr_{80-x}Al_xCu_{20}$ alloys

Zhe-Huan Jin(金哲欢)[1,2], Lei Jin(金磊)[1,2], Guang-Fei Ding(丁广飞)[2,3], Shuai Guo(郭帅)[2,3,†], Bo Zheng(郑波)[2], Si-Ning Fan(樊思宁)[2], Zhi-Xiang Wang(王志翔)[2], Xiao-Dong Fan(范晓东)[2], Jin-Hao Zhu(朱金豪)[2], Ren-Jie Chen(陈仁杰)[2,3,4], A-Ru Yan(闫阿儒)[2,3], Jing Pan(潘晶)[1], and Xin-Cai Liu(刘新才)[1,‡]

[1] *School of Materials Science and Chemical Engineering, Ningbo University, Ningbo* 315211, *China*

[2] *Key Laboratory of Magnetic Materials and Devices, Ningbo Institute of Materials Technology and Engineering, Chinese Academy of Sciences, Ningbo* 315201, *China*

[3] *University of Chinese Academy of Sciences, Beijing* 100049, *China*

[4] *Ganjiang Innovation Academy, Chinese Academy of Science, Ganjiang* 342799, *China*

(Received 2 January 2022; revised manuscript received 28 March 2022; accepted manuscript online 14 April 2022)

A grain boundary diffusion (GBD) process with $Pr_{80-x}Al_xCu_{20}$ ($x = 0$, 10, 15, 20) low melting point alloys was applied to commercial 42M sintered Nd–Fe–B magnets. The best coercivity enhancement of a diffused magnet was for the $Pr_{65}Al_{15}Cu_{20}$ GBD magnet, from 16.38 kOe to 22.38 kOe. Microstructural investigations indicated that increase in the Al content in the diffusion source can form a continuous grain boundary (GB) phase, optimizing the microstructure to enhance the coercivity. The coercivity enhancement is mainly due to the formation of a continuous GB phase to separate the main phase grains. Exchange decoupling between the adjacent main phase grains is enhanced after the GBD process. Meanwhile, the introduction of Al can effectively promote the infiltration of Pr into the magnet, which increases the diffusion rate of rare-earth elements within a certain range. This work provides a feasible method to enhance coercivity and reduce the use of rare-earth resources by partial replacement of rare-earth elements with non-rare-earth elements in the diffusion source.

Keywords: Nd–Fe–B, grain boundary diffusion, coercivity enhancement, grain boundary phase

PACS: 75.60.Nt, 75.50.Ww, 75.50.Vv, 75.60.Ej **DOI:** 10.1088/1674-1056/ac6741

1. Introduction

Nd–Fe–B permanent magnets are widely used in wind turbines and traction motors of electric/hybrid vehicles due to their excellent magnetic properties such as a high energy product. But the intrinsic coercivity deteriorates with increasing working temperature, which greatly limits high-temperature applications.[1,2] Therefore, the coercivity of Nd–Fe–B sintered magnets at room temperature should be enhanced to meet high-temperature requirements. Various attempts have been made to increase coercivity and retain the remanence (B_r) of sintered Nd–Fe–B magnets. It became clear that the coercivity of sintered Nd–Fe–B magnets is controlled by the nucleation of reversed magnetic domains on the surface of Nd–Fe–B main phase grains.[3] The grain boundary diffusion (GBD) process was then developed to enhance the anisotropy field at the magnet surface and the coercivity, in addition to reducing the cost of the final magnet.[4] Heavy rare-earth (HRE)-rich alloys were coated on the magnet surface followed by heat treatment, causing diffusion into the magnets along the grain boundary (GB) and forming a (Nd, Dy/Tb)$_2$Fe$_{14}$B hardened shell at the near surface layer to enhance the coercivity. However, the antiferromagnetic coupling of the HRE atoms and Fe atoms inevitably caused a decrease in the saturated magnetization M_S for the main phase grains.[5]

Recently, GBD process technology with HRE-free diffusion source has been developed to conserve HRE resources in response to the substantial price increase in heavy rare-earths. The properties can be enhanced effectively by microstructural optimization in HRE-free sintered magnets.[6,7] Magneto-optical Kerr effect microscopy analysis has shown that exchange-decoupled Nd–Fe–B sintered magnets with optimized microstructure can hinder the extension of the reversed magnetic domain and achieve better magnetic properties.[8] Therefore, for the GBD process it has been reported that $Nd_{70}Cu_{30}$,[9] Pr–Cu[10] and Pr–Al–Co[11] low melting point HRE-free eutectic alloys have been applied in sintered Nd–Fe–B magnets to modify the microstructure and enhance the properties. The enhancement of coercivity is mainly due to the formation of a continuous Nd-rich GB phase. Exchange decoupling between adjacent grains can be improved by microstructural optimization.[12] Further research found that coercivity enhancement can be influenced by the Al/Cu ratio in the diffusion source.[13] Besides, Al can improve the wettability of the GB phase to enhance the diffusion rate, while replacement of some of the Fe by Al can further improve coercivity, although the anisotropy field of the Nd–Fe–B sintered magnets decreases slightly.[14,15] Thus Al has been widely used in the design of the diffusion source. To enhance coercivity, the light

†Corresponding author. E-mail: gshuai@nimte.ac.cn

‡Corresponding author. E-mail: liuxincai@nbu.edu.cn

© 2023 Chinese Physical Society and IOP Publishing Ltd

rare-earth element Pr was chosen because the anisotropy field of $Pr_2Fe_{14}B$ is higher than that of $Nd_2Fe_{14}B$.[16] It has been reported that substitution of Nd by Pr in sintered Nd–Fe–B magnets cause the GBs to become clear and smooth.[17] Cu was chosen as the other component of the diffusion source because Al/Cu co-added alloy can effectively improve the mobility of the diffusion source over $Nd_2Fe_{14}B$ grains and enhance the coercivity.[15] In this work, we replaced a small amount of Pr with Al in the Pr–Al–Cu low melting point alloy diffusion source to carry out GBD for a good relative performance of the Nd–Fe–B sintered magnets. The effect of GB optimization is discussed based on the microstructure and the element distribution.

2. Experimental details

Commercial 42M HRE-free sintered Nd–Fe–B magnets of size 6 mm × 6 mm × 5 mm were prepared as the original magnets. Diffusion sources with compositions of $Pr_{80-x}Al_xCu_{20}$ (at.%; $x = 0$, 10, 15 and 20, named PC, PAC-10, PAC-15, and PAC-20, respectively) low melting point eutectic alloys were prepared by electric arc melting in an argon atmosphere. These alloys were then cut by wire-electrode cutting into flakes of size 6 mm × 6 mm × 0.2 mm for use as the diffusion sources. The flakes were polished with abrasive paper and cleaned in alcohol then put on the upper and lower surfaces of the magnets and placed in crucibles. Finally, the GBD process was carried out at 700 °C for 10 h with subsequent annealing at 500 °C for 2 h in a high-vacuum atmosphere. The magnetic properties of the original magnet and the diffused magnets were measured at various temperatures using a pulsed-field magnetometer (PFM14.CN). The backscattered electron (BSE) images and element distribution of the annealed magnets were observed by a scanning electron microscope (SEM; Quanta FEG 250) equipped with an energy dispersive spectrometer (EDS; Oxford INCA system). The compositions of the original magnet and PAC-15 GBD magnet obtained in this work were determined by induction coupled plasma optical electron spectroscopy (ICP).

3. Results and discussion

Figure 1(a) shows the room temperature demagnetization curves of the original and diffused magnets with $Pr_{80-x}Al_xCu_{20}$ alloys. The coercivity of the magnets was enhanced from 16.38 kOe to 17.67 kOe, 21.65 kOe, 22.38 kOe, and 21.51 kOe for the PC, PAC-10, PAC-15, and PAC-20 GBD magnets, respectively. The maximum percentage enhancement in coercivity H_{cj} was found for the PAC-15 GBD magnet, being 36.63% higher than that of the original magnet. Meanwhile, remanence B_r decreased from 13.37 kG to 12.82 kG, 12.74 kG, 12.69 kG, and 12.69 kG for the PC, PAC-10, PAC-15, and PAC-20 GBD magnets, respectively. The decrease in B_r was attributed to infiltration of the non-ferromagnetic phase. To further study the function of Al, figure 1(b) shows the magnetic properties of the diffused magnets with different Al contents. It can be clearly seen that H_{cj} increases enormously with increase of the Al content to 15 at.% compared with the PC GBD magnets, but H_{cj} decreases slightly with further increase in the Al content. In addition, B_r and $(BH)_{max}$ decrease continuously with increase in the Al content. Addition of Al to the diffusion source is beneficial for enhancing the coercivity of the diffused magnets. The coercivity enhancement may be caused by microstructural optimization.

For daily application in high-temperature conditions, the high-temperature properties of the GBD magnets are also crucial. Figure 2 summarizes the temperature dependence of remanence and coercivity from 20 °C to 160 °C for the original and $Pr_{80-x}Al_xCu_{20}$ GBD magnets. The temperature coefficients of remanence (α) and coercivity (β) were calculated according to the following formulae:

$$\alpha = \frac{B_r(T_2) - B_r(T_1)}{B_r(T_1)(T_2 - T_1)} \times 100\%,$$

$$\beta = \frac{H_{cj}(T_2) - H_{cj}(T_1)}{H_{cj}(T_1)(T_2 - T_1)} \times 100\%,$$

where T_2 is 120 °C, T_1 represents room temperature (20 °C), B_r (T_2) is the remanence at 120 °C, B_r (T_1) is the remanence at 20 °C, H_{cj} (T_2) is the coercivity at 120 °C and H_{cj} (T_1) is the coercivity at 20 °C. The coercivity coefficient (β) is enhanced from -0.6254 %·°C^{-1} to -0.6062 %·°C^{-1}. In addition, the remanence coefficient (α) is enhanced from -0.1399 %·°C^{-1} to -0.1240 %·°C^{-1} for the PAC-10 GBD magnet. However, the value of β decreased slightly when the Al content reached 20 at.%. It is interesting that the thermal stability of coercivity and remanence was not improved with an Al content of 15 at.% compared with the PAC-10 GBD magnet. This result suggests that the appropriate Al ratio in the diffusion source plays a critical role in the high-temperature properties of GBD magnets which can improve the high-temperature properties of the diffused magnets. However, the high-temperature properties will deteriorate with further increase in the Al content. Detailed coefficient values are listed in the top right corners of Figs. 2(a) and 2(b). To further compare individual magnetic properties of the original and PAC-10 GBD magnets at different test temperatures, detailed test values are listed in Table 1. From this table it is clearly seen that the coercivity of the original magnet decreased from 16.44 kOe at 20 °C to 3.96 kOe at 160 °C, while the coercivity of the PAC-10 GBD magnet decreased from 21.54 kOe at 20 °C to 5.16 kOe at 160 °C. Meanwhile, $(BH)_{max}$ of the PAC-10 GBD magnet is still higher than that of the original magnet at 160 °C, indicating that the diffused magnet can provide a higher energy for high-temperature applications.

Table 1. Magnetic properties of original and PAC-10 GBD magnets at 20 °C–160 °C.

T (°C)	Original magnet			PAC-10 GBD magnet		
	B_r (kG)	H_{cj} (kOe)	$(BH)_{max}$ (MG·Oe)	B_r (kG)	H_{cj} (kOe)	$(BH)_{max}$ (MG·Oe)
20	13.34	16.44	40.88	12.71	21.54	38.78
60	12.73	11.41	37.13	12.16	15.63	35.46
80	12.38	9.34	34.99	11.86	13.03	33.63
100	11.99	7.59	32.05	11.52	10.63	31.65
120	11.50	6.16	27.61	11.16	8.48	29.68
140	10.98	4.96	23.84	10.75	6.71	27.21
160	10.44	3.96	18.73	10.20	5.16	22.91

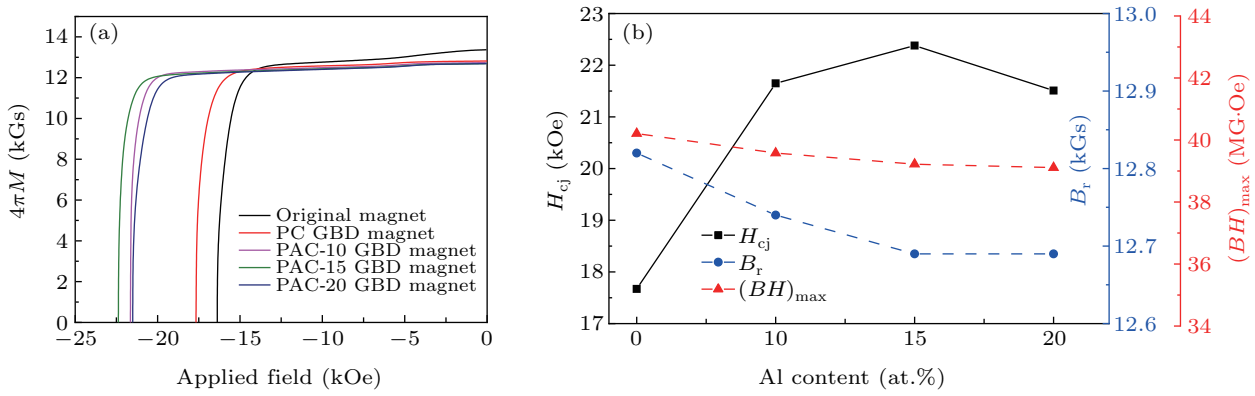


Fig. 1. (a) The room temperature demagnetization curves of the original magnet and the magnets diffused with the $Pr_{80-x}Al_xCu_{20}$ ($x = 0$, 10, 15, 20) alloys. (b) The properties of the original magnet and the magnets diffused with the $Pr_{80-x}Al_xCu_{20}$ ($x = 0$, 10, 15, 20) alloys.

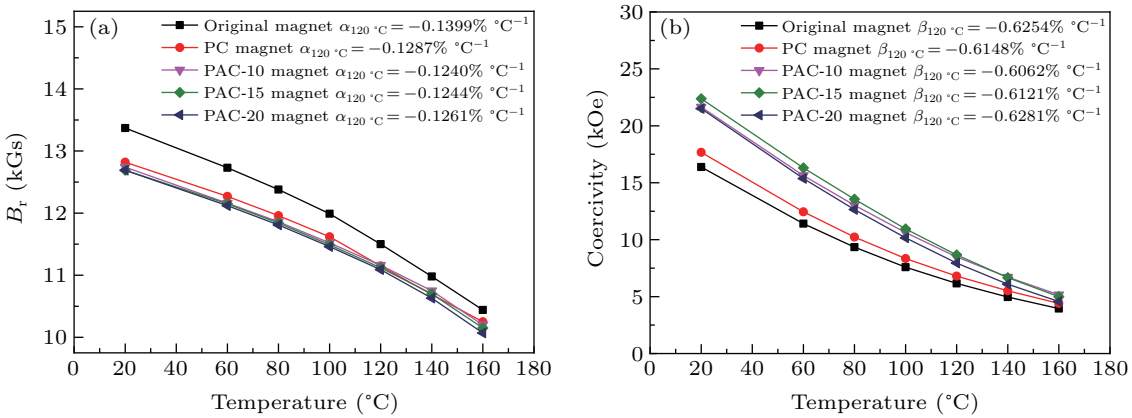


Fig. 2. Temperature-dependent properties of the original and $Pr_{80-x}Al_xCu_{20}$ diffused magnets: (a) remanence, (b) coercivity. The corresponding temperature coefficients are listed in the top right corners.

To observe the structural transformation of the diffused magnets, figure 3 shows BSE images of the $Pr_{80-x}Al_xCu_{20}$ GBD magnets at various depths. The dark region represents the Nd–Fe–B main phase grains and the white region represents the GB phase. In the PC GBD magnet, a Nd-rich phase exists in the form of a triple junction phase (TJP) for all diffusion depths. There is no obvious continuous GB phase; this is not conducive to demagnetization coupling between the adjacent main phase grains and thus excellent coercivity cannot be obtained. However, at 50 μm in the PAC-10, PAC-15, and PAC-20 GBD magnets, a continuous thin GB can be distinguished clearly along the main phase grains. This microstructure can effectively enhance the magnetic decoupling between the main phase grains and then increase the coercivity. Meanwhile, it is noted that a continuous GB phase is still not visible in the PAC-10, PAC-15, and PAC-20 GBD magnets even at 900 μm. It was worth noting that the thickness of the continuous thin GB phase at depths between 100 μm and 900 μm in the PAC-20 GBD magnets is wider than that of the PAC-10 GBD magnets. These results show that a diffusion source with Al can effectively promote the formation of the continuous GB phases compared with PC and PAC GBD magnets. The decreased remanence is not only caused by the increased GB phase but also by the partial replacement of Fe by Al in the matrix phase during the GBD process. However, the coercivity of the PAC-15 magnet has not been further enhanced. Thus it can be deduced that an appropriate Al content in the diffusion source can improve the coercivity by contributing to

microstructural optimization.

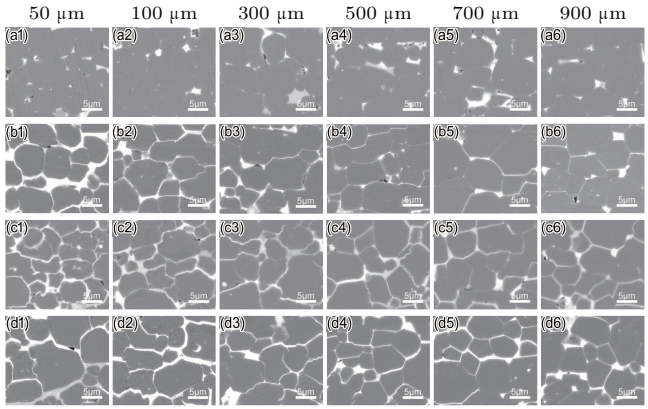


Fig. 3. Backscattered SEM images of the $Pr_{80-x}Al_xCu_{20}$ diffused magnets at various depths (50 μm–900 μm) from the surface: (a) $Pr_{80}Cu_{20}$, (b) $Pr_{70}Al_{10}Cu_{20}$, (c) $Pr_{65}Al_{15}Cu_{20}$, (d) $Pr_{60}Al_{20}Cu_{20}$.

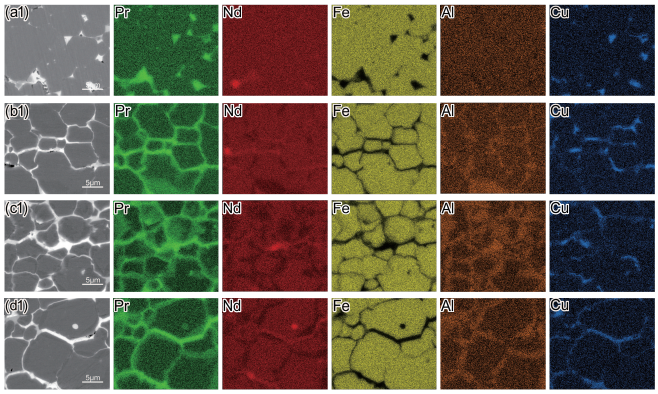


Fig. 4. Back-scattered SEM images of the $Pr_{80-x}Al_xCu_{20}$ diffused magnets at 100 μm — (a) PC, (b) PAC-10, (c) PAC-15, (d) PAC-20 — together with EDS elemental mappings of the corresponding area.

Figure 4 shows the microstructure and corresponding EDS Pr, Nd, Fe, Cu, and Al distribution maps at 100 μm from the surface of the magnets diffused by $Pr_{80-x}Al_xCu_{20}$ alloys. In the PC GBD magnet shown in Fig. 4(a) it can be seen that, judging by the EDS mappings, the TJPs are mainly aggregates of Pr and a small amount of Cu and Al. For PAC-15 GBD magnets, the $Nd_2Fe_{14}B$ main phase isolated by the continuous GB phase can be clearly distinguished. The GB phase is rich in Pr, Al and Cu elements due to the increase in Al content in the diffusion source. Al plays a role in improving the wettability of the GB phase during the diffusion process. In addition, the (Nd, Pr)$_2$Fe$_{14}$B shell on the outer layer of the main phase grains can also be observed. With further increases in the Al content in the diffusion source, the thickness of the (Nd, Pr)$_2$Fe$_{14}$B shell tends to increase. Meanwhile, the proportion of Al in the GB phase is increased. The gray contrast in the TJP can be distinguished; EDS analysis shows this to have the chemical composition $Pr_{21.43}Nd_{15.72}Fe_{49.90}Al_{8.31}Cu_{4.63}$ (at.%). The formation of this phase may be beneficial to coercivity enhancement. In addition, by comparing the Al element maps for the PAC-15 and PAC-20 GBD magnets, partial replacement of Fe by Al in the main phase grains can enhance H_{cj}. However, H_{cj} can decrease slightly as the Al content in the main phase continues to increase.

As mentioned in a previous study,[18] excessive accumulation of rare-earth elements in the surface and lack of a Nd-rich phase as a diffusion channel are not conducive to enhancement of the coercivity. In this work, coercivity enhancement is attributed to microstructural optimization which can be influenced by the diffusion coefficients of Pr and Al. Therefore, figure 5 shows the concentration distribution of Pr and Al determined by EDS analysis in the $Pr_{80-x}Al_xCu_{20}$ GBD magnets at various depths. The Pr concentration of the PC GBD magnet at 50 μm is only 4.14 at.%, much lower than the 8.90 at.% of the PAC-10 GBD magnet, the 9.63 at.% of the PAC-15 GBD magnet and the 8.78 at.% of the PAC-20 GBD magnet, indicating that the diffusion process cannot be facilitated without Al in the diffusion source. When the diffusion depth increases from 50 μm to 300 μm, the Pr concentration decreases to 4.79 at.%, 5.74 at.%, and 5.75 at.% for PAC-10, PAC-15 and PAC-20 GBD magnets, respectively. Meanwhile, the Al concentration also shows same tendency. However, we note that the Pr concentration in the PAC-15 diffusion source is lower than the PAC-10 diffusion source, but the PAC-15 GBD magnet has the largest Pr concentration at any diffusion depth. Thus, it can be deduced that Al has an effective role in promoting the infiltration of Pr into the magnet. This can explain why the room temperature coercivity of the PAC-15 GBD magnet is larger than that of the PAC-10 GBD magnet. This provided a reliable reason for the use of non-rare-earth elements to replace rare-earth elements in GBD. Nevertheless, the coercivity deteriorates slightly with further increase in the Al content in the diffusion source due to more Fe being replaced by Al.[19]

As shown above, the Al concentration of the PAC-15 GBD magnet at various depths is largest among all the GBD magnets. To quantitatively analyze the Pr concentration gradient influenced by Al in the diffusion process, the Pr profile follows Fick's second law with diffusion depth (x) and time (t), described as

$$c(x,t) = c_s - (c_s - c_0)\mathrm{erf}\left(\frac{x}{2\sqrt{Dt}}\right),$$

where c_s and c_0 are the surface concentration and the inside concentration, respectively, and D is the diffusion coefficient. To satisfy the requirement for block magnets, we selected the greatest distance ($x = 900$ μm) for calculation. The detailed data on the Pr diffusion coefficients obtained at 700 °C for various Al contents are listed in Table 2. These indicate definitively that Pr infiltration into the sintered magnets can be promoted by the introduction of Al within a certain range, and is beneficial in enhancing the coercivity of the block magnets. The diffusion coefficient of Pr is largest when the Al content

is 15 at.%. These data further support the SEM results on optimization of the microstructure and formation of a Pr-rich shell structure, and explain the reason for the coercivity enhancement.

Table 2. Grain boundary diffusion coefficients of Pr in different diffusion sources at 700 °C.

	PC	PAC-10	PAC-15	PAC-20
D_{Pr} (10^{-8} cm^2·s^{-1})	2.0242	2.2306	2.8213	2.4703

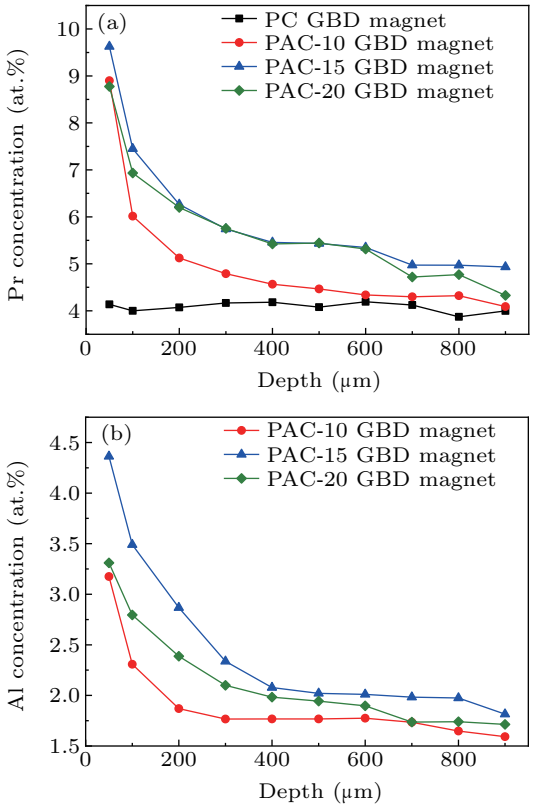


Fig. 5. The concentration distribution of Pr (a) and Al (b) in the $Pr_{80-x}Al_xCu_{20}$ diffused magnets at various depths from the surface.

The present experimental results provide a feasible guideline for the design of the diffusion source for sintered Nd–Fe–B magnets. Replacement of Pr in the diffusion source by the non-rare-earth element Al can reduce the use of rare-earth resources and enhance the coercivity, and is also beneficial in promoting infiltration of Pr into the sintered Nd–Fe–B magnets and improving utilization of rare-earth elements in the diffusion source.

Figure 6(a) summarizes rare-earth introduction, H_{cj} enhancement and B_r reduction in this work compared with Pr–Cu GB reconstruction and PrAl GBD. The concentration of the original magnet and PAC-15 GBD magnet in this work is $Pr_6Nd_{23.6}Fe_{bal}Cu_{0.1}Al_{0.5}M_{1.2}B_{0.95}$ (wt.%) and $Pr_{7.87}Nd_{22.16}Fe_{bal}Cu_{0.35}Al_{0.57}M_{1.2}B_{0.96}$ (wt.%) obtained by ICP testing. The rare-earth content has increased by 0.5 wt.%, while the coercivity has increased by 6 kOe (16.38 kOe to 22.38 kOe). Figure 6(a) summarizes the rare-earth increment, coercivity increment and B_r decrement of the GBD magnets from HRE-free eutectic alloys.[10,20] Compared with the values for the magnet with introduced $Pr_{83}Cu_{17}$ (wt.%) alloy reported by Tang *et al.*,[10] the coercivity increment of the $Pr_{65}Al_{15}Cu_{20}$ magnet in this work is higher than that of Pr–Cu diffused magnet with a low rare-earth increment. A magnet diffused by $Pr_{80}Al_{20}$ (at.%) alloy has been reported by Cao *et al.*[20] Although the increase in rare-earth content in Pr–Al diffused magnets is larger than in Pr–Al–Cu diffused magnets, the increase in coercivity in Pr–Al diffused magnets is lower than that in Pr–Al–Cu diffused magnets. Figure 6(b) shows the relationship between the coercivity enhancement and magnet thickness for Dy-containing powder and low melting point alloys.[9,13,21–25] By controlling the microstructure of the diffused magnets, the coercivity shows a great increase for a thickness of about 5 mm. The coercivity enhancement is equivalent to that of a 3 mm magnet diffused with Dy powder. Therefore, a higher coercivity is anticipated for PrAlCu-diffused magnets due to a combination of the introduction of rare-earths and magnet thickness.

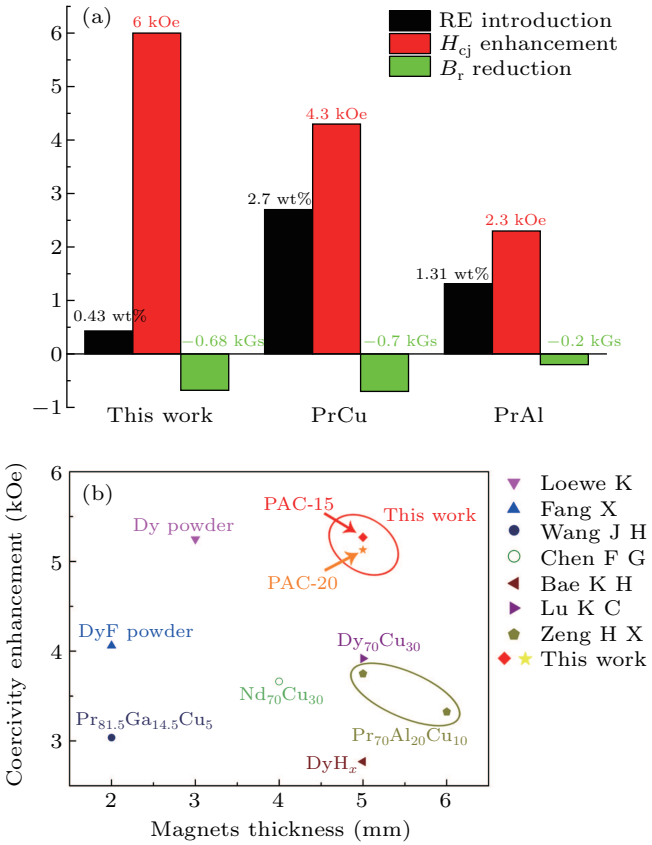


Fig. 6. (a) Comparisons of rare-earth introduction (black), H_{cj} enhancement (red) and B_r reduction (green) among PAC-15 ($Pr_{65}Al_{15}Cu_{20}$), $Pr_{68.77}Cu_{31.23}$, and $Pr_{80}Al_{20}$ (at.%) processed magnets. (b) Coercivity enhancement of the magnets diffused by PAC-15 ($Pr_{65}Al_{15}Cu_{20}$), PAC-20 ($Pr_{60}Al_{20}Cu_{20}$), DyF powder,[22] $Pr_{81.5}Ga_{14.5}Cu_5$,[23] Dy powder,[21] $Nd_{70}Cu_{30}$,[9] DyH,[24] $Dy_{70}Cu_{30}$,[25] and $Pr_{70}Al_{20}Cu_{10}$.[13]

4. Conclusion

In summary, 42M sintered magnets diffused with $Pr_{80-x}Al_xCu_{20}$ low melting point eutectic alloys have been

fabricated. The coercivity of the $Pr_{80-x}Al_xCu_{20}$ diffused magnets was enhanced from 16.38 kOe for the original magnet to 17.67 kOe, 21.65 kOe, 22.38 kOe, and 21.51 kOe for $x = 0$, 10, 15 and 20, respectively. The above results show that the best magnetic properties are obtained when $x = 15$. Combined with microstructural analysis of the PC and PAC-15 GBD magnets, the coercivity enhancement resulted from the enhancement of magnetic decoupling due to the formation of a continuous GB phase. The formation of a GB phase can effectively increase magnetic decoupling between the adjacent main phase grains. With further increase in the Al content in the diffusion source, all the magnetic properties of the PAC-20 GBD magnet decreased slightly. This is due to the infiltration of a lot of Al into the main phase grains. When the Al content is within a certain range, it benefits the infiltration of Pr into the magnet so as to enhance the coercivity according to the concentration–depth analysis. So, our work suggests that the replacement of an appropriate amount of Pr by Al in the diffusion source can be beneficial for improving the magnetic properties and reducing the use of rare-earth resources.

Acknowledgments

Project supported by the National Key Research and Development Program of China (Grant No. 2021YFB3502802), Major Science and Technology Research and Development Project of Jiangxi Province, China (Grant No. 20203ABC28W006), the Key Research and Development Program of Shandong Province, China (Grant No. 2019JZZY010321), Major Project of "Science and Technology Innovation 2025" in Ningbo City (Grant No. 2020Z046), and the K. C. Wong Magna Fund in Ningbo University.

References

[1] Hono K and Sepehri-Amin H 2012 *Scr. Mater.* **67** 530
[2] Brown D, Ma B M and Chen Z M 2002 *J. Magn. Magn. Mater.* **248** 432
[3] Fukagawa T, Hirosawa S, Ohkubo T and Hono K 2009 *J. Appl. Phys.* **105** 07A724
[4] Hirota K, Nakamura H, Minowa T and Honshima M 2006 *IEEE Trans. Magn.* **42** 2909
[5] Herbst J F 1991 *Rev. Mod. Phys.* **63** 819
[6] Ding G F, Liao S C, Di J H, Zheng B, Guo S, Chen R J and Yan A R 2020 *Acta Mater.* **194** 547
[7] Xu X D, Sasaki T T, Li J N, Dong Z J, Sepehri-Amin H, Kim T H, Ohkubo T, Schrefl T and Hono K 2018 *Acta Mater.* **156** 146
[8] Soderznik M, Sepehri-Amin H, Sasaki T T, Ohkubo T, Takada Y, Sato T, Kaneko Y, Kato A, Schrefl T and Hono K 2017 *Acta Mater.* **135** 68
[9] Chen F G, Zhang T Q, Wang J, Zhang L T and Zhou G F 2015 *Scr. Mater.* **107** 38
[10] Tang M H, Bao X Q, Zhang X J, Mu X, Lu K C, Li J H and Gao X X 2019 *J. Rare Earth.* **37** 393
[11] Jin L, Jin Z H, Zhu J H, Ding G F, Zheng B, Guo S, Chen R J, Yan A R and Liu X C 2021 *Chin. Phys. B* **30** 027503
[12] Zhu J H, Jin L, Jin Z H, Ding G F, Zheng B, Guo S, Chen R J and Yan A R 2021 *Chin. Phys. B* **30** 067503
[13] Zeng H X, Liu Z W, Li W, Zhang J S, Zhao L Z, Zhong X C, Yu H Y and Guo B C 2019 *J. Magn. Magn. Mater.* **471** 97
[14] Di J H, Ding G F, Tang X, Yang X, Guo S, Chen R J and Yan A R 2018 *Scr. Mater.* **155** 50
[15] Lu K C, Bao X Q, Chen G X, Zhang X J, Tang M H, Mu X, Li J H and Gao X X 2019 *Scr. Mater.* **160** 86
[16] Hirosawa S, Matsuura Y, Yamamoto H, Fujimura S, Sagawa M and Yamauchi H 1986 *J. Appl. Phys.* **59** 873
[17] Chen B C, Liu X M, Chen R J, Guo S, Lee D and Yan A R 2012 *J. Alloys Compd.* **516** 73
[18] Kim T H, Lee S R, Yun S J, Lim S H, Kim H J, Lee M W and Jang T S 2016 *Acta Mater.* **112** 59
[19] Hirosawa S, Yamaguchi Y, Tokuhara K, Yamamoto H, Fujimura S and Sagawa M 1987 *IEEE Trans. Magn.* **23** 2120
[20] Cao S, Bao X Q, Li J H, Yu H J, Zhu K Y and Gao X X 2020 *J. Rare Earth.* **38** 395
[21] Loewe K, Brombacher C, Katter M and Gutfleisch O 2015 *Acta Mater.* **83** 248
[22] Xu F, Wang J, Dong X P, Zhang L T and Wu J S 2011 *J. Alloys Compd.* **509** 7909
[23] Wang J H, Wang G and Zeng D C 2020 *J. Magn. Magn. Mater.* **503** 166639
[24] Bae K H, Kim T H, Lee S R, Kim H J, Lee M W and Jang T S 2014 *J. Alloys Compd.* **612** 183
[25] Lu K C, Bao X Q, Tang M H, Sun L, Li J H and Gao X X 2017 *J. Magn. Magn. Mater.* **441** 517